

MSAT – A new toolkit for the analysis of elastic and seismic anisotropy¹

Andrew M. Walker^{a,*} and James Wookey^a

^a*School of Earth Sciences, University of Bristol, Wills Memorial Building, Queen's
Road, Bristol, BS8 1RJ, UK*

Abstract

The design and content of MSAT, a new Matlab toolkit for the study and analysis of seismic and elastic anisotropy, is described. Along with a brief introduction to the basic theory of anisotropic elasticity and a guide to the functions provided by the toolkit, three example applications are discussed. First, the toolkit is used to analyse the effect of pressure on the elasticity of the monoclinic upper mantle mineral diopside. Second, the degree to which a model of elasticity in the lowermost mantle can be approximated by transverse isotropy is examined. Finally backazimuthal variation in the effective shear wave splitting caused by two anisotropic layers where the lower layer is dipping is calculated. MSAT can be freely reused for any purpose and the implementation of these and other examples are distributed with the source code.

Key words: MATLAB, anisotropy, shear-wave splitting, elasticity, seismology

* phone: +44 (0)117 9545245, fax: +44 (0)117 9253385

Email addresses: andrew.walker@bristol.ac.uk (Andrew M. Walker),
j.wookey@bristol.ac.uk (James Wookey).

¹ NOTICE: this is the author's version of a work that was accepted for publication in "Computers and Geosciences". Changes resulting from the publishing process,

1 Introduction

The observation and analysis of seismic anisotropy has become a powerful tool in global, industrial and environmental geophysics with applications as varied as the study of mantle convection (e.g. Savage, 1999; Panning and Romanowicz, 2004; Becker et al., 2012), subduction zones (e.g. Nakajima and Hasegawa, 2004; Morley et al., 2006; Di Leo et al., 2012) and other plate boundaries (e.g. Kosarin et al., 2011; Lin et al., 2011; Nowacki et al., 2012), continental and lithospheric structure (e.g. Silver and Chan, 1988, 1991; Bastow et al., 2010, 2011), hydrocarbon exploration and extraction (e.g. Kendall et al., 2007; Winterstein et al., 2001; Verdon and Kendall, 2011), and the monitoring of CO₂ storage sites (Verdon et al., 2011). Consequences of the anisotropic nature of the Earth include the splitting of S-waves into two perpendicularly polarised arrivals with different wave speeds (Crampin, 1984a), the variation in amplitude of reflected (Hall and Kendall, 2000) and converted waves (Vinnik et al., 2007) with direction, and, most simply, a variation in wave velocity with propagation direction (Hess, 1964). On the length-scales probed by seismology the anisotropy can arise from a variety of processes. These include the generation of aligned fractures (Hudson, 1981, 1980; Crampin, 1984b), solid or liquid filled inclusions (Tandon and Weng, 1984), sedimentary layering (Backus, 1962), or the alignment of crystals by solid state deformation (e.g. Wenk, 1999), growth from a melt (e.g. Bergman et al., 2005) or sedimentary deposition (Valcke et al., 2006). A large amount of information can thus be recovered by measur-

such as peer review, editing, corrections, structural formatting, and other quality control mechanisms may not be reflected in this document. Changes may have been made to this work since it was submitted for publication. A definitive version was subsequently published in *Computers and Geosciences*, [49 pp.81–90 (2012)]. <http://dx.doi.org/10.1016/j.cageo.2012.05.031>

ing and modelling the seismic consequences of anisotropy.

Since studies of seismic anisotropy rarely end with its measurement, modelling tools are needed to provide explanations for its physical origin and to yield useful geological or geophysical information. Seismic anisotropy reflects an underlying anisotropy in the elastic properties of the material through which the waves propagate. More than two elastic constants (e.g. the bulk and shear moduli) are needed to describe the relationship between stress and elastic strain. Indeed, in the most general case 21 distinct elastic moduli are needed to link the six components of the general stress tensor to the six components of the strain tensor or to calculate the velocities of seismic waves propagating through an anisotropic body. This makes software designed to handle anisotropic elasticity more complex than codes limited to the isotropic case but the cost of the added complexity can yield significant insight into the geological problem in hand. Here we describe a new Matlab toolbox, called MSAT, designed to aid the modelling needed for the interpretative step of the analysis of seismic anisotropy and to enable studies of elastic anisotropy more generally. Provision of key building blocks for modelling in this modern integrated development environment allows the rapid development and prototyping of explanations for measured anisotropy. The Matlab graphical environment also permits plotting of key anisotropic parameters. Furthermore, the software complements SplitLab (Wüstefeld et al., 2008) a Matlab environment used for measuring shear wave splitting and the MTEX toolbox (Bachmann et al., 2010; Mainprice et al., 2011) used for the analysis of textures in rocks.

The remaining parts of the paper are arranged as follows. In section 2 we review some of the key theoretical and mathematical concepts needed in order to model seismic and elastic anisotropy. Section 3 contains a description of

the design, implementation, availability, capability and contents of the MSAT toolbox. Three example applications of the software are given in section 4 and the paper closes with a concise summary and some ideas for further development.

2 Background theory

MSAT is concerned with linear elasticity, the continuum theory describing the relationship between stresses and small, instantaneous and recoverable strains. As a measure of internal force per-unit area, stress can be represented by a second rank tensor, σ . Having defined a Cartesian reference frame, a general stress in three dimensions can be described by three forces, each operating on the face normal to an axis of the reference frame and, in general, having three components (one normal to the face and two parallel to it). Denoting the orientations of the planes and directions of the components of the forces by two indices, the stress tensor can thus be represented as a nine-element matrix, σ_{ij} , which must be symmetric if the body is in equilibrium (is not accelerating). Strain measures material deformation and this can also be represented by a second rank tensor, $\varepsilon_{ij} = \frac{1}{2}(u_{i,j} + u_{j,i})$, where u represents a change in length along an axis and the comma indicates partial differentiation with respect to direction. This definition also results in a symmetric matrix. The fourth-order elastic constants (or stiffness) tensor, \mathbf{C} , allows the calculation of the stress required to produce a particular strain:

$$\sigma_{ij} = C_{ijkl}\varepsilon_{kl}, \tag{1}$$

where the repeated indices on the right hand side imply summation in this, and all similar equations. Similarly, if the stress is known the resulting strain can be calculated using the compliance tensor which (following the perverse logic of the stiffness tensor being labelled \mathbf{C}) is conventionally denoted \mathbf{S} :

$$\varepsilon_{ij} = S_{ijkl}\sigma_{kl}. \quad (2)$$

MSAT provides a range of functions for analysing and manipulating representations of elasticity and these are described below (section 3.2). Many of these contain implementations of different theories, however we will not reproduce these here: the reader is directed to the works referenced for that background. However, there are several pieces of theory which underpin several of the functions provided, which are worth covering briefly.

The first of these is the symmetry exhibited by the elastic constants tensor. The symmetry of the stress and strain tensors implies that $C_{ijkl} = C_{jikl}$ and $C_{ijkl} = C_{ijlk}$ (the *minor symmetries*). Furthermore, it turns out that the stiffness tensor can be written as a function of the second derivative of the internal energy, U , with strain:

$$C_{ijkl} = \frac{\partial^2 U}{\partial \varepsilon_{ij} \partial \varepsilon_{kl}}, \quad (3)$$

and this results in the *major symmetries*: $C_{ijkl} = C_{klij}$. Taken together these symmetry relations reduce the 81 constants relating 9 stresses to 9 strains to 21 distinct constants relating 6 stresses to 6 strains and these arguments apply equally to \mathbf{S} . For convenience, elastic constants are usually representation using Voigt notation. This represents the 4th order tensor C_{ijkl} as a symmetric 6×6

matrix $C_{\alpha\beta}$ (with no loss of information), where:

$$\begin{array}{cccccc}
 ij \text{ or } kl : & & 11 & 22 & 33 & 32 = 23 & 31 = 13 & 12 = 21 \\
 \downarrow & \downarrow & & & & & & & \\
 \alpha & \beta & 1 & 2 & 3 & 4 & 5 & 6 & \cdot \quad (4)
 \end{array}$$

It is a convenient property of the Voigt notation \mathbf{C} matrix that the equivalent compliance matrix \mathbf{S} can be found by simple matrix inversion. Note, however, that the compliance matrix cannot be treated quite like the elastic stiffness, for example the conversion between the 4th order tensor representation and the Voigt matrix form includes additional factors for the compliance.

In the most general case discussed above, 21 elastic constants are required to represent minerals with a triclinic symmetry (such as, for example, albite), but crystals with a higher symmetry (e.g. orthorhombic, hexagonal or cubic) require fewer elastic constants. In the simplest case — that of isotropic materials — this reduces to the two Lamé coefficients λ and μ . The reader is directed to, for example, Babůska and Cara (1991) or Mainprice (2007) for a detailed discussion of the forms of the elastic matrix for different symmetry classes. The limitations of what can usually be resolved using seismology mean that higher symmetry classes are often assumed. A class which is commonly invoked is transverse isotropy (TI, also known as radial or polar anisotropy, see, e.g., Thomsen, 1986). In a TI medium properties only vary with angle from the symmetry axis. This can arise in a number of ways and is exhibited by: crystalline materials with a hexagonal symmetry, isotropic thin layers of different stiffness (e.g., Backus, 1962), aligned inclusions (e.g., Tandon and

Weng, 1984) or cracks which are uniformly oriented (e.g., Hudson, 1980, 1981). TI requires five independent constants to parameterise. There are a number of commonly used choices of parameter sets (depending on the area of literature); MSAT has functions to work with several of these.

The second key piece of background concerns the rotation of elastic constants tensors. Recall that a vector, \mathbf{v} is rotated from to a new orientation, $\mathbf{v}^{(R)}$, by multiplication by a rotation matrix: $\mathbf{v}^{(R)} = \mathbf{g}\mathbf{v}$, where the rotation matrix, \mathbf{g} , is a 3×3 orthogonal matrix with determinant 1 and elements that represent the cosines of angles of the rotation. This transformation be also be written element-wise as: $v_i^{(R)} = g_{ij}v_j$ (with an implicit summation over $j = 1, 3$). This formula can be extended for higher order Cartesian tensors. For example, the second order stress tensor is rotated: $\sigma_{ij}^{(R)} = g_{ik}g_{jl}\sigma_{kl}$ (with two implicit summations) and the elastic stiffness tensor rotated: $C_{ijkl}^{(R)} = g_{im}g_{jn}g_{kp}g_{lq}C_{mnpq}$ (with four summations and avoiding Voigt notation). For second order tensors the transformation can also be written in the form of matrix multiplication by the rotation matrix and its transpose: $\sigma^{(R)} = \mathbf{g}\sigma\mathbf{g}^T$, but this shortcut is not available for higher order tensors. However, it is possible (in fact, highly desirable for performance reasons) to perform rotations on elastic constants in Voigt form without requiring to transform to the $3 \times 3 \times 3 \times 3$ tensor form. In order to do this we use the formula from Bond (1943, Equation 8.9):

$$\mathbf{C}^{(R)} = \mathbf{K} \mathbf{C} \mathbf{K}^T \quad (5)$$

where $\mathbf{C}^{(R)}$ is the rotated version of \mathbf{C} . In this equation \mathbf{K} is a 6×6 matrix derived from combinations of the normal 3×3 rotation matrix and \mathbf{K}^T is its matrix transpose. See Bower (2009, Section 3.2.11), Winterstein (1990, page

1075) or Bond (1943, Equation 7.2) for details. We note in passing that the derived matrices for anticlockwise rotation around the principle axes presented by Bower contain a number of sign errors (a common pitfall when dealing with rotation matrices!). For reference, the corrected form of these matrices are:

$$\begin{array}{c}
 \left| \begin{array}{cccccc}
 1 & 0 & 0 & 0 & 0 & 0 \\
 0 & c^2 & s^2 & -2cs & 0 & 0 \\
 0 & s^2 & c^2 & 2cs & 0 & 0 \\
 0 & cs & -cs & c^2 - s^2 & 0 & 0 \\
 0 & 0 & 0 & 0 & c & s \\
 0 & 0 & 0 & 0 & -s & c
 \end{array} \right| \left| \begin{array}{cccccc}
 c^2 & 0 & s^2 & 0 & 2cs & 0 \\
 0 & 1 & 0 & 0 & 0 & 0 \\
 s^2 & 0 & c^2 & 0 & -2cs & 0 \\
 0 & 0 & 0 & c & 0 & -s \\
 -cs & 0 & cs & 0 & c^2 - s^2 & 0 \\
 0 & 0 & 0 & s & 0 & c
 \end{array} \right| \left| \begin{array}{cccccc}
 c^2 & s^2 & 0 & 0 & 0 & -2cs \\
 s^2 & c^2 & 0 & 0 & 0 & 2cs \\
 0 & 0 & 1 & 0 & 0 & 0 \\
 0 & 0 & 0 & c & s & 0 \\
 0 & 0 & 0 & -s & c & 0 \\
 cs & -cs & 0 & 0 & 0 & c^2 - s^2
 \end{array} \right|
 \end{array} \quad (6)$$

where $s = \cos \theta$ and $c = \sin \theta$, for rotation around the 1-, 2- and 3- axes respectively. MSAT, however, only uses the general form of the K matrix to allow arbitrary rotations.

Another technique which underlies many of the routines concerns the averaging of elastic constants. In geophysics we are rarely dealing with single crystals. We need, therefore, a method of estimating the aggregate elastic properties of a polycrystalline material containing a range of crystal types and orientations. While much more rigorous treatments exist (see, e.g., Mainprice, 2007, for an overview) for many purposes simple averaging schemes suffice. These either assume constant strain (Voigt averaging) or stress (Reuss averaging) throughout the sample, and essentially amount to taking the arithmetic average of each element of the stiffness or compliance tensor, respectively. These

two values place an upper (Voigt) and lower (Reuss) bound on the true value. It was observed by Hill (1952) that experimental values were often close to the average of these two bounds, a value which has become known as the Voigt-Reuss-Hill (VRH) average:

$$C^{\text{VRH}} = \frac{1}{2} (C^{\text{Voigt}} + C^{\text{Reuss}}) \quad (7)$$

where

$$C^{\text{Voigt}} = \sum_{i=1}^N v_i C_i \quad \text{and} \quad C^{\text{Reuss}} = \left[\sum_{i=1}^N v_i S_i \right]^{-1}. \quad (8)$$

Here, v_i are the volume fractions of the N individual components, with associated elasticities (C_i) and compliances (S_i). This is very commonly employed in geophysics and mineral physics, and is implemented in `MS_VRH` in `MSAT`. It should be noted that it is an empirical relation with no strict theoretical foundation, albeit a useful one.

Finally, `MSAT` also concerns itself with determining seismic properties from elastic media. The propagation of motion through an elastic medium is governed by the elastodynamics equation:

$$\rho \left(\frac{\partial^2 u_i}{\partial t^2} \right) = C_{ijkl} \left(\frac{\partial^2 u_l}{\partial x_j \partial x_k} \right) \quad (9)$$

where ρ is the density, u_i is the displacement, x_j is position and t is time. By substituting into this the displacement associated with a monochromatic plane wave as a function of time, we obtain the well-known Christoffel equation:

$$\left(C_{ijkl} n_j n_l - \rho V^2 \delta_{ik} \right) p_k = 0 \quad (10)$$

where n_j is the propagation unit vector, V are the phase velocities, p_k are

the polarisation unit vectors and δ_{ik} is the Kronecker delta function. Solutions to this equation for a given direction (n_j) yield the three orthogonal waves with different phase velocities. One of these will be close to the wavefront normal (designated quasi-P or qP) and two will be near perpendicular (quasi-S1, quasi-S2; qS1 and qS2). In practice the quasi- prefix is often omitted. The reader is directed to Mainprice (2007) for a more complete treatment of the subject. MSAT follows the methodology of Mainprice (1990) to calculate phase velocities (see `MS_phasevels`).

3 Software

In order to facilitate the analysis and modelling of observations of seismic and elastic anisotropy we have developed a new Matlab toolbox, called MSAT (the Matlab Seismic Anisotropy Toolbox) described below. We chose to write MSAT in Matlab for a number of reasons including the language's adoption by many geophysicists, its portability and the ease of generation of graphical output. A major strength of Matlab is in the integration of powerful tools for linear algebra and the manipulation of two-dimensional matrices. We therefore use the convenient and compact Voigt matrix representation of anisotropic elasticity and always represent the elasticity as a rank-two size 6×6 Matlab array. In the rest of this work and in the MSAT documentation we choose call these arrays *elasticity matrices* to avoid confusion with the rank-four elastic stiffness and elastic compliance tensors.

3.1 Design, development and documentation

We developed MSAT using modern tools with ease of use and maintenance in mind. One important choice involved the way data is represented and functions accessed. Matlab offers facilities for libraries to provide an object oriented interface — a design which, for MSAT, would imply the creation of elasticity objects associated with crystals or rocks with functions accessed as methods belonging to these objects. We chose instead to provide a simple procedural interface to the library as, in our experience, few seismologists who make use of Matlab (our target audience) make use of the relatively recent object oriented facilities offered by the language. In order to avoid some of the difficulties with namespace ambiguity we impose a common naming convention and argument ordering to the MSAT functions. All function names begin with `MS_` and argument lists typically begin with the elasticity matrix followed by the density.

A second important aspect of usability is accessible documentation. We have followed the Matlab convention and provide documentation via two routes. Firstly, the source code of each function contains a comment block describing what the function does and how it should be used. We have provided this documentation consistently and always provide key references to the literature and cross-references to related functions. The Matlab system displays this documentation in the command window when the built-in `help` function is used. The second source of documentation adds a short “getting started” document, a longer “user guide” and detailed usage examples. These, together with the function descriptions, are accessible using the Matlab documentation browser. This documentation is also available on the web. In order to help

avoid the situation where documentation and code drift out of sync, we have built a simple system to create much of this documentation from the comment blocks in the code. When modifying function behaviour the author (or code reviewer) only needs to ensure text in the same file as the modified source code is updated.

In creating MSAT we made use of two modern development tools we consider essential in order to ease development, future enhancement and maintenance. We provide a test harness and a set of functionality and regression tests driven by the `xunit` toolbox². These tests cover almost all the accessible functions (except the plotting functions, which are difficult to test automatically) and provide an easy way to quickly identify the presence of new errors from the Matlab development environment. We expect new tests will be created to cover new functionality or to prevent regressions if particular defects are discovered in the future. In order to allow rapid, independent and parallel development by multiple authors we made use of `git`, an advanced distributed version control system.³ A web-accessible view of this system, which includes access to the whole development history, can be accessed online alongside a database to handle reports of bugs and enhancement requests.⁴

3.2 Functions

MSAT provides 27 functions designed to be used together to build tools to analyse elastic and seismic anisotropy. In describing the basic features of the

² <http://www.mathworks.com/matlabcentral/fileexchange/22846-matlab-xunit-test-framework>

³ <http://git-scm.com/>

⁴ <https://github.com/andreww/MSAT>

toolkit we group the functions together according to how elasticity matrices appear in the lists of input or output arguments. In the first group of functions elasticity matrices are created from the input arguments (Table 1). `MS_load` and `MS_load_list` simply read data from input files (several data formats are supported) while `MS_elasticDB` extracts elasticity information from a database included with the distribution. Other functions create elasticity matrices from summary information and a knowledge of the symmetry. For example, `MS_iso` builds an isotropic elasticity matrix from the P- and S-wave velocities and density while `MS_TI` creates a matrix with transverse isotropy and a vertical symmetry axis given, for example, the Thomsen parameters (Thomsen, 1986).

It is also possible to model the effective anisotropic elasticity caused by particular rock fabrics; an effect that can be important even if all the components of the rock are isotropic on a short length scale compared to the seismic wavelength. For example, if an elastically isotropic medium contains aligned ellipsoidal inclusions filled with an elastically isotropic material of a different stiffness the effective elasticity is anisotropic. When the inclusions are axially symmetric the net effect is the creation of transverse isotropy (Tandon and Weng, 1984). A similar effect can arise from layering of isotropic materials of different stiffness (Backus, 1962). This is a common occurrence in sedimentary basins where the beds have distinct lithology and thus elastic properties. The `MS_effective_medium` function allows the creation of elasticity matrices representing these cases.

The second group of functions include elasticity matrices as input and output. These functions, listed in Table 2, are used to manipulate or transform an elasticity matrix. Simple examples of these functions are `MS_rot3`, `MS_rotEuler`

and `MS_rotR`, which rotate an elasticity matrix (the functions differ in the way the rotation is specified). `MS_axes` also rotates an input matrix but by an amount designed to allow the anisotropic nature of the matrix to be analysed. Such analysis makes use of two other functions, `MS_decomp` and `MS_norms`. Taken together, these three functions allow the symmetry of elasticity matrices to be expressed following the approach of Browaeys and Chevrot (2004) and an example of this approach is given below (Section 4.2). Finally, `MS_VRH` calculates the Voigt, Reuss, and Voigt-Reuss-Hill average elasticity of an aggregate of materials, each described by their own elasticity matrix and volume fraction, while `MS_polyaverage` takes this averaging one step further and estimates the isotropic elasticity matrix if the components are randomly oriented.

MSAT's third group of functions (Table 3) allow elasticity to be analysed or displayed. They take elasticity matrices as input arguments and either return derived quantities or cause graphics to be produced. Examples include `MS_anisotropy`, which implements some of the attempts to capture the degree of elastic anisotropy of a material as a single value (Ledbetter and Miglion, 2006; Ranganathan and Ostoja-Starzewski, 2008) and `MS_poisson` which calculates Poisson's ratio for a general anisotropic material as a function of direction (Wojciechowski, 2005). `MS_phasevels` solves the Christoffel equation for given propagation directions and returns the three seismic phase velocities along with their polarisations. This function is used by `MS_plot` and `MS_sphere`, which plot the resulting seismic anisotropy on a pole figures and a three-dimensional spherical representation, respectively (see Section 4.1).

Finally, a few utility functions are also provided (Table 4), which are commonly used internally by MSAT. These include `MS_cij2cijkl` and `MS_cijkl2cij`, which convert between Voigt and full tensor notation of elasticity. `MS_checkC`

confirms that an elasticity matrix is in the form expected by MSAT and is physically meaningful.

3.3 Availability

The MSAT code and documentation along with access to key development tools is available online.⁵ The code has been tested using Matlab versions between 2009b and 2012a but we do not expect issues running on other systems. MSAT is distributed with a three-clause BSD license and can thus be freely used, and redistributed, on a commercial or non-commercial basis. We encourage users to report any potentially useful changes or enhancements they may make along with reports of difficulties, bugs and requests for new features.

4 Applications

MSAT can be used for applications in mineral physics and materials science in addition to seismology. As well as being useful for data analysis and modelling the toolbox can be used as an aid for rapidly prototyping more involved applications that will eventually be implemented outside of the Matlab development environment. In this section we provide three brief examples of the kind of applications that MSAT enables. These are chosen to demonstrate usage for the analysis of single-crystal elasticity data, the calculation and analysis of the effective elasticity of deformed polycrystalline samples, and modelling of shear wave splitting. The source code associated with these examples is distributed along with the toolkit.

⁵ <http://www1.gly.bris.ac.uk/MSAT>

4.1 *Analysis of single crystal elasticity*

By themselves, a set of single crystal elastic constants from an experiment or atomic scale simulation are of limited use to the geophysicist. This is especially true for low symmetry systems where the link between the elasticity matrix and properties such as degree of anisotropy or seismic wave speeds can be disguised by the arithmetic complexity. In this example, we show how MSAT can be used to illuminate the way that the elasticity of diopside, a monoclinic upper mantle mineral, changes with pressure. The raw data is derived from atomic scale calculations making use of density functional theory (Walker, 2012) and covers pressures from 0 to 20 GPa.

The evolution of the individual elastic constants with pressure is shown in Figure 1 a and b. Whether seen graphically or in a table of numbers one major feature stands out: most of the elastic constants increase with increasing pressure. Careful examination shows that some constants decrease with increasing pressure but without additional computation it is impossible to tell if the anisotropy increases or decreases or how the pattern of seismic anisotropy changes. As shown in Listing 1, we can use MSAT to evaluate the degree of anisotropy as a function of pressure using either the universal anisotropy index proposed by Ranganathan and Ostoja-Starzewski (2008) or the general measure of anisotropy suggested by Ledbetter and Miglione (2006); both are suitable for monoclinic symmetry. The result, shown in Table 5, is that pressure has the effect of decreasing the elastic anisotropy of diopside.

The decrease in measures of the overall elastic anisotropy does not necessarily imply that the observed seismic anisotropy will decrease with pressure. In

the mantle a possible mechanism for the generation of seismic anisotropy is the tendency for the crystal lattices of a material undergoing plastic deformation to align. This leads to the formation of a lattice (or crystallographic) preferred orientation. The seismic anisotropy as a function of propagation direction through a single crystal becomes interesting as this is the maximum possible anisotropy that could be generated by this process (e.g. Figure 1 c–e). Deformed rocks containing diopside often have the diopside crystals aligned such that the (010) plane is parallel to the shear direction. For horizontal upper mantle shear and near vertical wave propagation directions (e.g. SKS phases) it is therefore instructive to consider the shear wave splitting expected for propagation in the [010] direction in diopside. As shown in Table 5 and Figure 1 this increases from 5.5% to 19.0% over the 0–20 GPa pressure range, while the measures of overall anisotropy decrease.

4.2 Polycrystal anisotropy

The lowermost layer of the lower mantle exhibits unusually high seismic anisotropy (Lay and Young, 1991; Vinnik et al., 1995; Kendall and Silver, 1996; Montagner and Kennett, 1996). Among the explanations for this observation is the development of a lattice preferred orientation in (Mg,Fe)SiO₃ post-perovskite. If this hypothesis is correct, it offers the possibility of accessing lower-mantle dynamics from the observation of seismic anisotropy (e.g. Panning and Romanowicz, 2004; Merkel et al., 2007). In an attempt to test this idea, Walker et al. (2011) simulated the development of post-perovskite LPO in the lowermost mantle by combining a tomography-based models of whole mantle convection (Forte, 2007; Simmons et al., 2007, 2009) with models of polycrys-

talline deformation (Lebensohn and Tomé, 1993). The initial output of these simulations are sets of crystal orientations (500 Euler angle triples) at each sampled point in the lowermost mantle and these were converted into polycrystalline elastic constants by forming the Voigt-Reuss-Hill mean of single crystal post-perovskite elasticity for each orientation (an example of this kind of calculation is provided with MSAT). In order to compare this elastic model (which assumes no particular symmetry) with global anisotropic tomography (Panning and Romanowicz, 2006; Panning et al., 2010; Kustowski et al., 2008), Walker et al. (2011) then imposed VTI symmetry on the model. In this example we show how the appropriateness of this approximation when compared to the full anisotropic model can be assessed.

The fragment of source code shown in Listing 2 shows one way to assess how close the general elastic model is to exhibiting hexagonal symmetry. The calculation, which has been repeated for each point in the global model, makes use of the decomposition method of Browaeys and Chevrot (2004). In MSAT this is achieved in three steps: first the elasticity matrix is rotated such that the principle directions of the stress tensor needed to produce an isotropic dilatation are aligned with the cartesian reference frame. This aligns symmetry elements with the cartesian frame. Then the (rotated) matrix is projected onto the orthogonal subspace representing each symmetry class. Finally, the Euclidean norm of the tensor for each class are calculated. This gives a measure of the relative contribution of each symmetry class to the initial generally isotropic tensor (see Browaeys and Chevrot, 2004, for further details). The results of this analysis are shown in Figure 2 along with the universal anisotropy index. As can be seen, the proportion of hexagonally is not well correlated with the overall anisotropy: regions with strongly non-hexagonal anisotropy (red in

Figure 2 a) can exhibit both large and small overall anisotropy (Figure 2 b). However, over the majority of the globe more than 70% of the norm of the elasticity can be described with an hexagonal approximation.

4.3 Modelling shear wave splitting

Shear-wave splitting is a well known effect of an anisotropic medium on the passage of a seismic wave through it (Crampin, 1984a). This is the separation of the shear wave into two orthogonal pulses, the orientation of which are determined by the medium's symmetry. These two waves propagate at different speeds, and so become separated in time. The delay and orientation of the pulses persist after the wave packet has exited the medium, and can be measured at the surface in three component seismic data (e.g., Ando et al., 1980; Vidale, 1986; Silver and Chan, 1988). Shear wave splitting is generally parameterised by polarisation angle (ϕ) and the delay time between the two pulses (δt), sometimes referred to together as the splitting operator (denoted Γ).

Probably the most common type of study of regional seismic anisotropy analyses shear-wave splitting in SKS/SKKS (core transiting teleseismic shear-wave phases, e.g., Silver and Chan, 1988, 1991; Savage, 1999). This has been used extensively to study anisotropy in many tectonic regimes. Other teleseismic phases (such as S and ScS) have been used extensively to study the deeper mantle (such as D'', see Nowacki et al., 2011, for a recent review).

A common situation inferred in SKS/SKKS studies is the presence of multiple layers of anisotropy in the mantle beneath the station. While each layer

causes the seismic wave to split, the frequency is generally too low to identify four individual wave pulses. Instead, an effective splitting is observed (denoted Γ_{EFF}) which is a combination of the individual operators and a function of the initial wave polarisation with respect to the medium fast directions (e.g., Silver and Savage, 1994). Thus, multiple layers are often inferred from the presence of a variation of the splitting operator with backazimuth. If layers also dip, the variation with backazimuth can be highly complex. While proper waveform modelling is required to completely understand the effects of complex anisotropy – and more robust modelling inversion methods are preferable (e.g., Abt and Fischer, 2008; Wookey, 2012) – considerable insight can be gained from simple models. The MSAT toolset provides methods for rapidly developing such models for a wide range of circumstances. For example, splitting operators for anisotropic models with a range of mechanisms, orientations and strengths can be calculated with `MS_phasevels`. Multiple operators can then be combined with the equations of Silver and Savage (1994), implemented in `MS_effective_splitting`.

An example of such a model is distributed with the code (`split_model`, see Listing 3). This uses the aforementioned methods to model the effect of two layers of aligned olivine on the observation of shear wave splitting in a near-vertically propagating phase (at a slowness similar to SKS). Figure 3 shows the geometry of the model, and Figure 4 shows the output generated. This demonstrates the variation of splitting parameters with source polarisation (which corresponds to backazimuth for SKS which is polarised by its conversion at the core-mantle boundary) for various values of the control parameters (orientation and dip of the layers). The mild variations of the individual splitting parameters associated with each layer combine to predict large effects

on the observed effective splitting. While the dip influences the results, the strongest effect comes from the interaction between the orientation of the two layers with respect to the polarisation.

5 Summary

We have described a Matlab toolkit designed to simplify the analysis and modelling of elastic and seismic anisotropy. This is fully documented and is freely reusable on a commercial and non-commercial basis. Notable components include the consistent implementation of a range of effective medium theories, tools to rotate, combine, decompose and summarise elasticity matrices, and functions to calculate parameters relating to seismic wave propagation such as shear wave splitting. In the examples above we have shown how this toolbox can be used to analyse single crystal elasticity, the seismic anisotropy of a polycrystalline aggregate, and backazimuthal variation of shear wave splitting generated by two dipping layers. Further example applications are distributed with the toolkit. Potential future enhancements which could be built into new versions of MSAT include the implementation of additional effective media theories (e.g. for layers of elastically anisotropic material) or of better approximations of the effect of multiple anisotropic regions along a seismic ray-path.

6 Acknowledgments

We are grateful to a large number of people who have shared code and insight on elastic and seismic anisotropy over the years, particularly David Mainprice and Mike Kendall. We also thank colleagues and collaborators who have tested

and commented on earlier versions of MSAT. This work has received funding from the European Research Council under the European Unions Seventh Framework Programme (FP7/2007-2013) / ERC Grant agreement n° 240473 “CoMITAC”.

References

- Abt, D. L., Fischer, K. M., 2008. Resolving three-dimensional anisotropic structure with shear wave splitting tomography. *Geophysical Journal International* 173, 859 – 886.
- Ando, M., Ishikawa, Y., Wada, H., 1980. S-wave anisotropy in the upper mantle under a volcanic area in Japan. *Nature* 286, 43 – 46.
- Babüska, V., Cara, M., 1991. *Seismic Anisotropy in the Earth*. Vol. 10 of *Modern Approaches in Geophysics*. Kluwer Academic Publishers, Dordrecht, Netherlands, 224 pp.
- Bachmann, F., Hielscher, R., Schaeben, H., 2010. Texture analysis with MTEX – free and open source software toolbox. *Solid State Phenomena* 160, 63 – 68.
- Backus, G. E., 1962. Long-wave elastic anisotropy produced by horizontal layering. *Journal of Geophysical Research* 67, 4427 – 4440.
- Bastow, I. D., Pilidou, S., Kendall, J.-M., Stuart, G. W., 2010. Melt-induced seismic anisotropy and magma assisted rifting in Ethiopia: Evidence from surface waves. *Geochemistry Geophysics Geosystemso* 11, Q0AB05.
- Bastow, I. D., Thompson, D., Wookey, J., Kendall, J.-M., Helffrich, G., Snyder, D., Eaton, D., Darbyshire, F. A., 2011. Precambrian plate tectonics: Seismic evidence from northern Hudson Bay, Canada. *Geology* 39, 91 – 94.
- Becker, T. W., Lebedev, S., Long, M. D., 2012. On the relationship between

- azimuthal anisotropy from shear wave splitting and surface wave tomography. *Journal of Geophysical Research* 117, B01306.
- Bergman, M. I., MacLeod-Silberstein, M., Haskel, M., Chandler, B., Akpan, N., 2005. A laboratory model for solidification of earth's core. *Physics of the Earth and Planetary Interiors* 153, 150 – 164.
- Bond, W. L., 1942. The mathematics of the physical properties of crystals. *The Bell System Technical Journal* 22, 1 – 72.
- Bower, A. F., 2009. *Applied mechanics of solids*. CRC Press, Boca Raton, Florida, USA.
 URL http://books.google.co.uk/books?id=1_sCzMNZMEsC
- Browaeyns, J. T., Chevrot, S., 2004. Decomposition of the elastic tensor and geophysical applications. *Geophysical Journal International* 159, 667 – 678.
- Chung, D. H., Buessem, W. R., 1967. The Voigt–Reuss–Hill approximation and elastic moduli of polycrystalline MgO, CaF₂, β -ZnS, ZnSe, and DdTe. *Journal of Applied Physics* 38, 2535 – 2540.
- Cowin, S. C., Mehrabadi, M. M., 1987. On the identification of material symmetry for anisotropic elastic materials. *Quarterly Journal of Mechanics and Applied Mathematics* 40, 451 – 476.
- Crampin, S., 1984a. An introduction to wave-propagation in anisotropic media. *Geophysical Journal of the Royal Astronomical Society* 76, 17 – 28.
- Crampin, S., 1984b. Effective anisotropic elastic constants for wave propagation through cracked solids. *Geophysical Journal of the Royal Astronomical Society* 76, 135 – 145.
- Di Leo, J. F., Wookey, J., Hammond, J. O. S., Kendall, J.-M., Kaneshima, S., Inoue, H., Yamashina, T., 2012. Deformation and mantle flow beneath the sangihe subduction zone from seismic anisotropy. *Physics of the Earth and Planetary Interiors* 194-195, 38 – 54.

- Forte, A. M., 2007. Constraints on seismic models from other disciplines – implications for mantle dynamics and composition. In: Romanowicz, B., Dziewonski, A. (Eds.), *Treatise on Geophysics. Seismology and the Structure of the Earth*. Vol. 1. Elsevier, pp. 805 – 858.
- Hall, S. A., Kendall, J.-M., 2000. Constraining the interpretation of AVOA for fracture characterisation. In: Ikelle, L., Gangi, A. (Eds.), *Anisotropy 2000: Fractures, Converted Waves, and Case Studies*. SEG, pp. 107 – 144.
- Hess, H., 1964. Seismic anisotropy of the uppermost mantle under oceans. *Nature* 203, 629–631.
- Hill, R., 1952. The elastic behaviour of a crystalline aggregate. *Proceedings of the Physics Society A* 65, 349 – 354.
- Hudson, J. A., 1980. Overall properties of a cracked solid. *Mathematical Proceedings of the Cambridge Philosophical Society* 88, 371 – 384.
- Hudson, J. A., 1981. Wave speeds and attenuation of elastic waves in material containing cracks. *Geophysical Journal of the Royal Astronomical Society* 64, 133 – 150.
- Kendall, J.-M., Fisher, Q. J., Covey Crump, S., Maddock, J., Carter, A., Hall, S. A., Wookey, J., Valcke, S. L. A., Lloyd, G. E., Ben Ismail, W., 2007. Seismic anisotropy as an indicator of reservoir quality in siliciclastic rocks. In: Jolley, S. J., Barr, D., Walsh, J. J., Knipe, R. J. (Eds.), *Structurally Complex Reservoirs*. Vol. 292 of Special Publication. Geological Society of London, pp. 123–136.
- Kendall, J.-M., Silver, P. G., 1996. Constraints from seismic anisotropy on the nature of the lowermost mantle. *Nature* 381, 409 – 412.
- Kosarin, M., Davis, P. M., Tanimoto, T., Clayton, R. W., 2011. The relationship between upper mantle anisotropic structures beneath California, transpression, and absolute plate motions. *Journal of Geophysical Research*

- 116, B08307.
- Kustowski, B., Ekström, G., Dziewoński, 2008. Anisotropic shear-wave velocity structure of the Earth's mantle: a global model. *Journal of Geophysical Research* 113, B06306.
- Lay, T., Young, C. J., 1991. Analysis of seismic SV waves in the core's penumbra. *Geophysical Research Letters* 18, 1373–1376.
- Lebensohn, R. A., Tomé, C. N., 1993. A self-consistent anisotropic approach for the simulation of plastic deformation and texture development of polycrystals: Application to zirconium alloys. *Acta Metallurgica et Materialia* 41 (9), 2611 – 2624.
- Ledbetter, H., Miglion, A., 2006. A general elastic-anisotropy measure. *Journal of Applied Physics* 100, 063516.
- Lin, F.-C., Ritzwoller, M. H., Yang, Y., Moschetti, M. P., Fouch, M. J., 2011. Complex and variable crustal and uppermost mantle seismic anisotropy in the western United States. *Nature Geoscience* 4, 55 – 61.
- Love, A. E. H., 1927. *A Treatise on the Theory of Elasticity* (4th Ed.). Cambridge University Press, Cambridge, UK, 643 pp.
- Mainprice, D., 1990. A fortran program to calculate seismic anisotropy from the lattice preferred orientation of minerals. *Computers and Geosciences* 16, 385 – 393.
- Mainprice, D., 2007. Seismic anisotropy of the deep earth from a mineral and rock physics perspective. In: Price, G. D. (Ed.), *Treatise on Geophysics. Mineral Physics. Vol. 2*. Elsevier, pp. 437 – 491.
- Mainprice, D., Hielscher, R., Schaeben, H., 2011. Calculating anisotropic physical properties from texture data using the MTEX open-source package. In: Prior, D. J., Rutter, E. H., Tatham, D. J. (Eds.), *Deformation Mechanisms, Rheology and Tectonics: Microstructures, Mechanics and Anisotropy. Vol.*

- 360 of Special Publication. The Geological Society of London, pp. 175 – 192.
- Merkel, S., McNamara, A. K., Kubo, A., Speziale, S., Miyagi, L., Meng, Y., Duffy, T. S., Wenk, H.-R., 2007. Deformation of (Mg,Fe)SiO₃ post-perovskite and D” anisotropy. *Science* 316, 1729 – 1732.
- Montagner, J.-P., Kennett, B. L. N., 1996. How to reconcile body-wave and normal-mode reference Earth models. *Geophysical Journal International* 125, 229 – 248.
- Morley, A. M., Stuart, G. W., Kendall, J.-M., Reyners, M., 2006. Mantle wedge anisotropy in the Hikurangi subduction zone, central North Island, New Zealand. *Geophysical Research Letters* 33, L05301.
- Nakajima, J., Hasegawa, A., 2004. Shear-wave polarization anisotropy and subduction-induced flow in the mantle wedge of northeastern Japan. *Earth and Planetary Science Letters* 225, 365 – 377.
- Nowacki, A., Kendall, J.-M., Wookey, J., 2012. Mantle anisotropy beneath the Earth’s mid-ocean ridges. *Earth and Planetary Science Letters* 317 - 318, 65 – 67.
- Nowacki, A., Wookey, J., Kendall, J.-M., 2011. New advances in using seismic anisotropy, mineral physics and geodynamics to understand deformation in the lowermost mantle. *Journal of Geodynamics* 52, 205 – 228.
- Panning, M., Romanowicz, B., 2004. Inferences on flow at the base of Earth’s mantle based on seismic anisotropy. *Science* 303, 351 – 353.
- Panning, M., Romanowicz, B., 2006. A three-dimensional radially anisotropic model of shear velocity in the whole mantle. *Geophysical Journal International* 167, 361 – 379.
- Panning, M. P., Lekić, V., Romanowicz, B. A., 2010. Importance of crustal corrections in the development of a new global model of radial anisotropy. *Journal of Geophysical Research* 115, B12325.

- Ranganathan, S. I., Ostoja-Starzewski, M., 2008. Universal elastic anisotropy index. *Physical Review Letters* 101, 055504.
- Savage, M. K., 1999. Seismic anisotropy and mantle deformation: What have we learned from shear wave splitting? *Reviews of Geophysics* 37, 65 – 106.
- Silver, P. G., Chan, W. W. J., 1988. Implications for continental structure and evolution from seismic anisotropy. *Nature* 335, 34 – 39.
- Silver, P. G., Chan, W. W. J., 1991. Shear-wave splitting and subcontinental mantle deformation. *Journal of Geophysical Research* 96, 16429 – 16454.
- Silver, P. G., Savage, M. K., 1994. The interpretation of shear-wave splitting parameters in the presence of 2 anisotropic layers. *Geophysical Journal International* 119, 949 – 963.
- Simmons, N. A., Forte, A. M., Grand, S. P., 2007. Thermochemical structure and dynamics of the African superplume. *Geophysical Research Letters* 34, L02301.
- Simmons, N. A., Forte, A. M., Grand, S. P., 2009. Joint seismic, geodynamic and mineral physical constraints on three-dimensional mantle heterogeneity: Implications for the relative importance of thermal versus compositional heterogeneity. *Geophysical Journal International* 177, 1284 – 1304.
- Tandon, G. P., Weng, G. J., 1984. The effect of aspect ratio of inclusions on the elastic properties of unidirectionally aligned composites. *Polymer Composites* 5, 327 – 333.
- Thomsen, L., 1986. Weak elastic anisotropy. *Geophysics* 51, 1954 – 1966.
- Valcke, S. L. A., Casey, M., Lloyd, G. E., Kendall, J.-M., Fisher, Q. J., 2006. Lattice preferred orientation and seismic anisotropy in sedimentary rocks. *Geophysical Journal International* 166, 652 – 666.
- Verdon, J. P., Kendall, J.-M., 2011. Detection of multiple fracture sets using observations of shear-wave splitting in microseismic data. *Geophysical*

- Prospecting 59, 593 – 608.
- Verdon, J. P., Kendall, J.-M., White, D. J., Angus, D. A., 2011. Linking microseismic event observations with geomechanical models to minimise the risks of storing CO₂ in geological formations. *Earth and Planetary Science Letters* 305, 143 – 152.
- Vidale, J. E., 1986. Complex polarization analysis of particle motion. *Bulletin of the Seismological Society of America* 76, 1393 – 1405.
- Vinnik, L., Romanowicz, B., Le Stunff, Y., Makeyeva, L., 1995. Seismic anisotropy in the D'' layer. *Geophysical Research Letters* 22, 1657 – 1660.
- Vinnik, L. P., Aleshin, I. M., Kiselev, S. G., Kosarev, G. L., Makeyeva, L. I., 2007. Depth localized azimuthal anisotropy from SKS and P receiver functions: The Tien Shan. *Geophysical Journal International* 169, 1289 – 1299.
- Walker, A. M., 2012. The effect of pressure on the elastic properties and seismic anisotropy of diopside and jadeite from atomic scale simulation. *Physics of the Earth and Planetary Interiors* 192-193, 81 – 89.
- Walker, A. M., Forte, A. M., Wookey, J., Nowacki, A., Kendall, J.-M., 2011. Elastic anisotropy of D'' predicted from global models of mantle flow. *Geochemistry Geophysics Geosystems* 12, Q10006.
- Walker, A. M., Tyer, R. P., Bruin, R. P., Dove, M. T., 2008. The compressibility and high pressure structure of diopside from first principles simulation. *Physics and Chemistry of Minerals* 35, 359 – 366.
- Wenk, H.-R., 1999. A voyage through the deformed earth with the self-consistent model. *Modelling and Simulation in Materials Science and Engineering* 7, 699 – 722.
- Winterstein, D. F., 1990. Velocity anisotropy terminology for geophysics. *Geophysics* 55, 1070 – 1088.
- Winterstein, D. F., De, G. S., Meadows, M. A., 2001. Twelve years of vertical

- birefringence in nine-component VSP data. *Geophysics* 66, 582 – 597.
- Wojciechowski, K. W., 2005. Poisson's ratio of anisotropic systems. *Computational Methods in Science and Technology* 11, 73 – 79.
- Wookey, J., 2012. Direct probabilistic inversion of shear-wave data for anisotropy. *Geophysical Journal International*In press.
- Wüstefeld, A., Bokelmann, G., 2007. Null detection in shear-wave splitting measurements. *Bulletin of the Seismological Society of America* 97, 1204 – 1211.
- Wüstefeld, A., Bokelmann, G., Zaroli, C., Barruol, G., 2008. SplitLab: A shear-wave splitting environment in Matlab. *Computers and Geosciences* 34, 515 – 528.
- Zenner, C., 1948. *Elasticity and Anelasticity of Metals*. University of Chicago Press.

Function name	Description and notes
<code>MS_build_isotropic</code>	Create elasticity matrix from pairs of isotropic moduli.
<code>MS_TI</code>	Generate elastic constants for a vertically transverse isotropic medium from Thomsen parameters (Thomsen, 1986), the ξ , ϕ and η parameters sometimes used in global scale tomography (e.g., Panning and Romanowicz, 2006), or the A, C, F, L , and N parameters of Love (1927). Symmetry is in the 3-axis in all cases.
<code>MS_effective_medium</code>	Generate elastic constants from various effective medium theories. Includes isotropic media containing ellipsoidal inclusions (Tandon and Weng, 1984), cracked (Hudson, 1980, 1981; Crampin, 1984b) and layered (Backus, 1962) media.
<code>MS_elasticDB</code>	Database of various elastic constants.
<code>MS_expand</code>	Fill out an elasticity matrix using symmetry.
<code>MS_iso</code>	Generate elasticity matrix from isotropic P- and S-wave velocities and density.
<code>MS_load</code>	Load an elasticity matrix from a file.
<code>MS_load_list</code>	Load a list of elasticity matrices from a file.

Table 1

MSAT functions for the input or generation of elasticity matrices. All return at least one elasticity matrix

Function name	Description and notes
<code>MS_VRH</code>	N-phase Voigt-Reuss-Hill average of elasticity.
<code>MS_axes</code>	Reorient elasticity matrix for optimal decomposition using method of Cowin and Mehrabadi (1987) and Browaeys and Chevrot (2004).
<code>MS_decomp</code>	Browaeys and Chevrot (2004) decomposition of the elasticity matrix.
<code>MS_polyaverage</code>	Calculate elasticity matrix for an isotropic polycrystal given the anisotropic single crystal matrix.
<code>MS_rot3</code>	Rotate elasticity matrix around three orthogonal axes.
<code>MS_rotEuler</code>	Rotate an elasticity matrix given Bunges convention for Euler angles.
<code>MS_rotR</code>	Use a rotation matrix to rotate an elasticity matrix.

Table 2

MSAT functions for the manipulation or transformation of elasticity matrices. All accept at least one elasticity matrix as an input argument and return at least one matrix as output.

Function name	Description and notes
<code>MS_anisotropy</code>	Measures of anisotropy defined by Zenner (1948), Chung and Buessem (1967), Ledbetter and Miglion (2006) and Ranganathan and Ostoja-Starzewski (2008).
<code>MS_norms</code>	Browaeys and Chevrot (2004) analysis of the elasticity matrix.
<code>MS_phasevels</code>	Calculate wave velocities in anisotropic media (Mainprice, 1990).
<code>MS_plot</code>	Plot wave velocities and anisotropy pole figures.
<code>MS_poisson</code>	Poisson's ratio in anisotropic media (Wojciechowski, 2005).
<code>MS_sphere</code>	Plot a spherical plot of wave velocities or anisotropy from a set of elastic constants.

Table 3

MSAT functions for the analysis and visualisation of elasticity matrices. These functions all accept at least one elasticity matrix as input but do not return elasticity as part of the output.

Function name	Description and notes
MS_checkC	Check consistency of an elasticity matrix against various criteria (must be a positive definite 6×6 symmetric Matlab array of real numbers).
MS_info	Report information about an elasticity matrix.
MS_cij2cijkl	Convert between an elasticity matrix (Voigt notation) and a rank-four array (full tensor).
MS_cijkl2cij	Convert a rank-four elasticity tensor (rank-four) to an elasticity matrix (Voigt notation).
MS_Vrot3	Rotate a three-vector.
MS_rotM	Create a rotation matrix.

Table 4
MSAT utility functions.

P	ρ	K	G	V_{Piso}	V_{Siso}	A^U	A^*	V_{qS1}	V_{qS2}	aV_S
GPa	kg/m ³	GPa	GPa	km/s	km/s	-	-	km/s	km/s	%
0.0	3276	124.3	71.7	8.4	4.9	0.5	1.9	5.0	4.8	5.5
5.0	3401	147.6	77.8	9.2	5.5	0.4	1.9	5.2	4.9	6.4
10.0	3512	169.2	82.6	9.9	6.1	0.4	1.9	5.4	4.8	11.5
15.0	3612	190.6	88.4	10.5	6.5	0.3	1.8	5.5	4.9	12.4
20.0	3704	208.8	88.7	11.0	7.0	0.3	1.7	5.6	4.6	19.0

Table 5
Properties derived from the elasticity of diopside as a function of pressure, P . The density ρ is taken from Walker et al. (2008) while the elastic constants are from Walker (2012). Calculated derived quantities include: the bulk, K , and shear, G , moduli of isotropic polycrystalline aggregates and their P- and S-wave velocities V_{Piso} and V_{Siso} ; the universal, A^U , and general, A^* , anisotropy indices of Ledbetter and Miglion (2006) and Ranganathan and Ostoja-Starzewski (2008), respectively; S-wave velocities, V_{qS1} and V_{qS2} , and anisotropy, $aV_S = (V_{qS1} - V_{qS2}) / \frac{1}{2}(V_{qS1} + V_{qS2})$, for waves propagating in the [010] direction.

```

1 % Loop over pressures , r(i) is the density , C(:,:,i)
2 % is the elasticity matrix
3 for i = 1:length(P)
4     % Calculate anisotropy index
5     [ uA, lmA ] = MS_anisotropy( C(:,:,i) );
6     % Calculate isotropic elasticity
7     [ K_vrh, G_vrh ] = MS_polyaverage( C(:,:,i) );
8     % Get isotropic phase velocities
9     Ciso = MS_build_isotropic( 'lam', G_vrh, 'K', K_vrh);
10    [ ~, ~, VSiso, ~, VPiso ] = MS_phasevels( Ciso, ...
11                                             r(i), 0.0, 0.0 );
12    % Calculate splitting for [010] direction (5km layer)
13    % This is along the y axis.
14    [ ~, aVS, VS1, VS2, ~ ] = MS_phasevels( C(:,:,i), ...
15                                             r(i), 0.0, 90.0 );
16    dt = (10/Vs2 - 10/Vs1);
17    % Write results for this pressure
18    fprintf(format_string, P(i), r(i), K_vrh, G_vrh, ...
19            VPiso, VSiso, uA, lmA, VS1, VS2, aVS);
20 end

```

Listing 1: Part of the source code used to extract anisotropic and seismic parameters from the elasticity of diopside. A full working version of this simple example is distributed with MSAT. The elasticity matrix, $C(:,:,i)$ and density, $r(i)$, corresponding to each pressure, $P(i)$ is analysed in turn for degree of anisotropy (line 5), elasticity of an isotropic aggregate (lines 7-11), and seismic wave speeds and shear-wave splitting magnitude (lines 14-16). Values printed by line 18 are reported in Table 5

```

1 % Rotate to optimum orientation
2 ChereR = MS_axes(Chere) ;
3 % Decompose into components
4 [C_iso , C_hex , C_tet , C_ort , C_mon , C_tri] = MS_decomp(ChereR) ;
5 % Calculate norms of components
6 P = MS_norms(ChereR , C_iso , C_hex , C_tet , C_ort , C_mon , C_tri) ;
7 % Hexagonal as a fraction of total anisotropic components
8 SumA = sum(P(2:end)) ;
9 PercH(ila(i) , ilo(i)) = P(2)./SumA ;

```

Listing 2: Part of the source code used to analyse the lowermost mantle model showing how the decomposition approach of Browaeys and Chevrot (2004) is implemented. The elasticity matrix at a point **Chere** is first rotated to allow optimum decomposition (line 2) then the rotated matrix is decomposed into isotropic, hexagonal, tetragonal, orthorhombic, monoclinic and triclinic components (line 3). The strength of each component is calculated (line 6; P is a length 6 array) and the fraction of the total anisotropic component of the elasticity matrix with hexagonal symmetry calculated (lines 8 and 9). A full working version of this example is distributed with MSAT and the result of this calculation shown in Figure 2 a

```

1 % interrogate elasticities to generate
2 % splitting parameters for each layer.
3 % (MS_phasevels is vectorised)
4 [ pol, ~, vs1, vs2, ~, ~, ~ ] = ...
5     MS_phasevels( L1_C, rh, inc, baz ) ;
6 % convert to geog. reference frame
7 fast1 = MS_unwind_pm_90((baz - pol')) ;
8 tlag1 = dist1./vs2' - dist1./vs1' ;
9
10 [ pol, ~, vs1, vs2, ~, ~, ~ ] = ...
11     MS_phasevels( L2_C, rh, inc, baz ) ;
12 fast2 = MS_unwind_pm_90((baz - pol')) ;
13 tlag2 = dist2./vs2' - dist2./vs1' ;
14
15 % Calculate the effective splitting
16 % between 2 layers (need to loop
17 % over propagation directions)
18 fast_eff = zeros(size(baz)) ;
19 tlag_eff = fast_eff ;
20 for i = 1:length(baz)
21     [ fast_eff(i), tlag_eff(i)] = ...
22         MS_effective_splitting_N(0.125, ...
23             baz(i), [fast2(i) fast1(i)], ...
24             [tlag2(i) tlag1(i)]) ;
25 end

```

Listing 3: Part of the source code used to calculate the effective splitting parameters of the model illustrated in Figure 3. The anisotropic elasticity of the two layers is described by `L1_C` and `L2_C` and the range of wave propagation directions is described by two arrays of angles, the back azimuth (`baz`) and the inclination (`inc`). Splitting parameters for the two layers are calculated using `MS_phasevels` (lines 1-13) then combined using `MS_effective_splitting_N` (lines 15-25). The remaining portions of the example (not shown) set up the geometry of the model, the elasticity matrices, and report the model output in textural and graphical form.

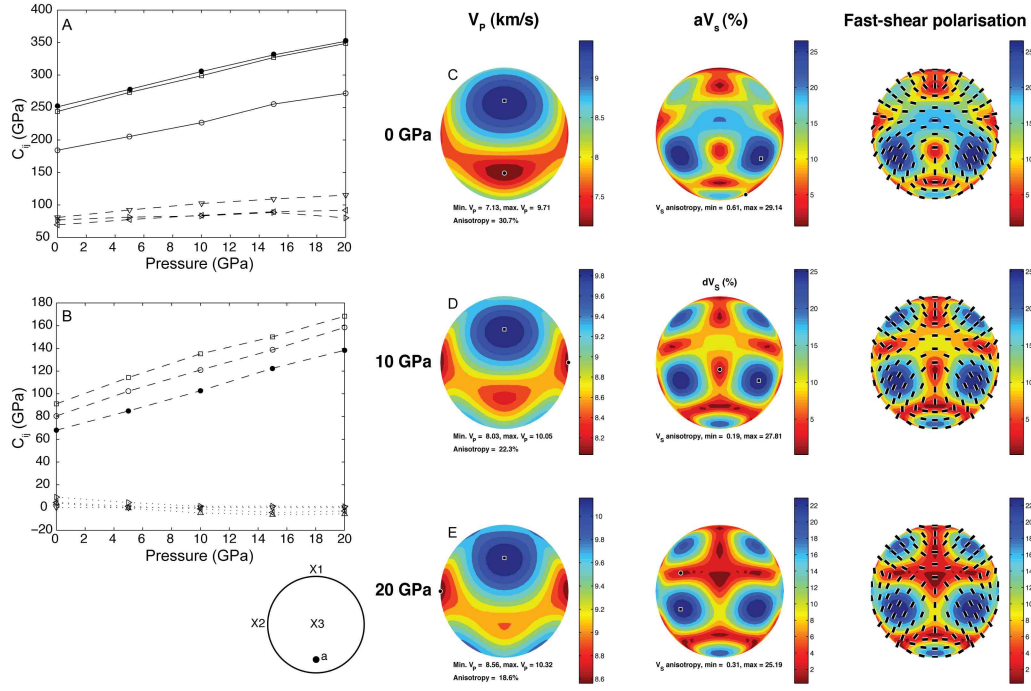


Fig. 1. Elasticity and phase velocities of diopside as a function of pressure. Parts (a) and (b) show the evolution of elements of the elasticity matrix with pressure as calculated using density functional theory. (In part (a): squares: C_{11} , unfilled circles: C_{22} , filled circles: C_{33} right pointing triangle: C_{44} , left pointing triangle: C_{55} , downwards pointing triangle: C_{66} . In part (b) squares: C_{12} , unfilled circles: C_{13} , filled circles: C_{23} , right pointing triangles: C_{15} , left pointing triangles: C_{25} , downwards pointing triangles: C_{65} , upwards pointing triangles: C_{43} .) Contours in parts (c), (d) and (e) show the variation in the velocity of the qP (left column) and difference in the velocity of the qS1 and qS2 phases (centre and right column) with propagation direction (upper hemisphere pole figures created with `MS_plot` with the cartesian axis system and approximate location of the crystallographic a axis shown in the inset) and pressure. Tick marks in the right hand column indicate the polarisation direction of the fast shear wave (qS1).

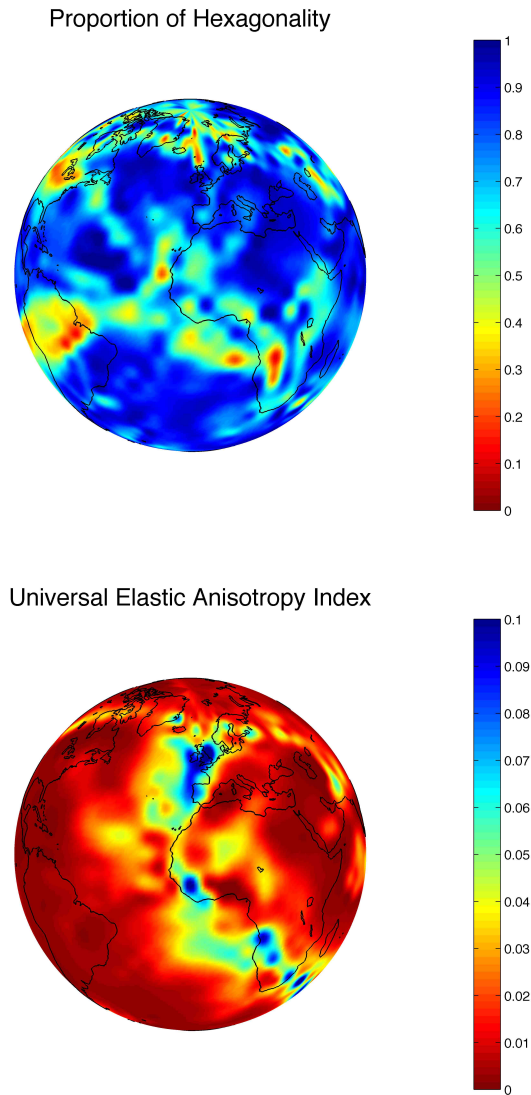


Fig. 2. Classifications of models of lowermost mantle anisotropy. Both panels show variations in properties extracted from a combined flow and texture model of the D'' (Walker et al., 2011). The upper panel shows the proportion of the predicted anisotropy which is captured by an assumption of vertical transverse isotropy (VTI). The lower panel shows the universal anisotropy index of Ranganathan and Ostoja-Starzewski (2008). The proportion of hexagonality is not well correlated with the overall anisotropy. However, over the majority of the globe more than 70% of the norm of the elasticity can be described with an hexagonal approximation.

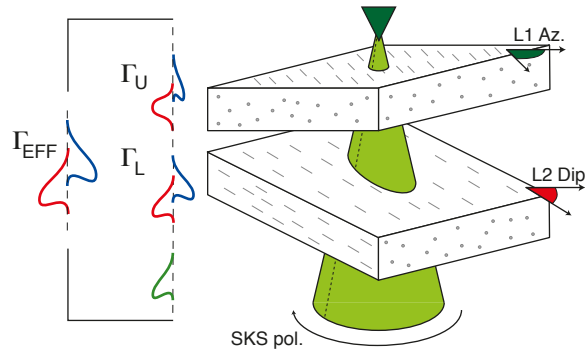


Fig. 3. Cartoon of the model encapsulated in the demonstration program `split_model`. This explores the effect of different orientation and dips of aligned olivine layers on the backazimuthal variation of shear wave splitting in SKS phases. Two layers (L1 and L2, with L1 uppermost) consisting of pure olivine with 30% crystal alignment, 50 km and 60 km thick respectively are included. The orientation of the texture in the upper layer (denoted L1 Azimuth) is varied, as is the dip beneath horizontal in the lower (denoted L2 Dip). The model is interrogated from all directions (the green cone denotes the surface swept out by the range of raypaths) corresponding to a set of source polarisations. For each angle a shear wave splitting operator is calculated for each layer (Γ_L and Γ_U). These are combined using the equations of Silver and Savage (1994) to produce the resultant splitting operator (Γ_{EFF}).

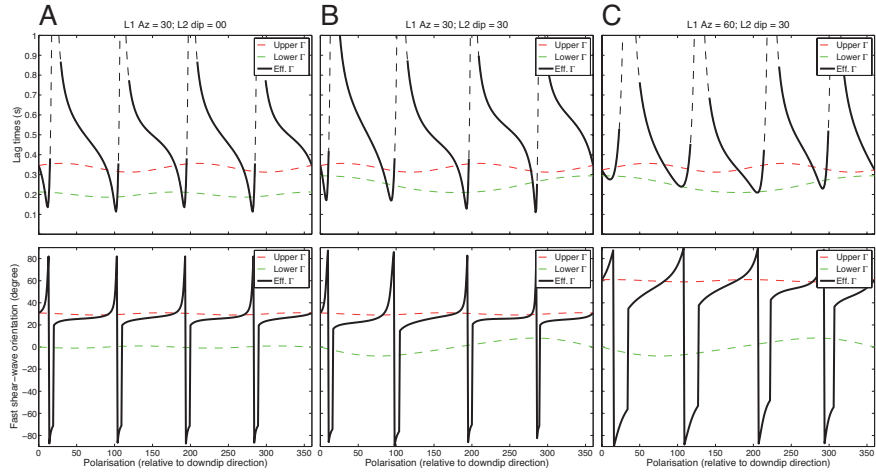


Fig. 4. Results of running the demonstration program `split_model`. This shows the variation of the splitting parameters (δt and ϕ in the upper and lower panels respectively) with respect to source polarisation calculated using the model shown in figure 3. Three cases are shown: A, L1 Azimuth = 30, L2 Dip = 0; B, L1 Azimuth = 30, L2 Dip = 30; and C, L1 Azimuth = 60, L2 Dip = 30. The individual layer parameters are shown in the red and green dashed lines, the black line shows the effective splitting. The dashed part of the black lines are where the effective fast direction is nearly parallel or perpendicular to the source polarisation. This would result in a null result in real data (Wüstefeld and Bokermann, 2007), and the effective splitting equations are unstable in such cases. While the dip influences the results (compare panels A and B), the strongest effect comes from the interaction between the orientation of the two layers with respect to the polarisation (compare panels B and C). The MSAT toolkit can be used to quickly implement and test simple models like these.